Program Digest, 2019 IEEE International Ultrasonics Symposium (IUS)
Glasgow, Scotland, October 6-9, 2019

Influence of Langasite Crystal Orientation on Hydrogen Gas Detection up to 400°C

Armando Ayes
Frontier Institute for Research in Sensor Technologies
Dept. of Electrical and Computer Engineering
University of Maine
Orono ME, USA
armando.ayes@maine.edu

Mauricio Pereira Da Cunha
Frontier Institute for Research in Sensor Technologies
Dept. of Electrical and Computer Engineering
University of Maine
Orono ME, USA
mdacunha@maine.edu

***Abstract*—Hydrogen gas sensors are of great importance due to the explosive nature and volatility of H_2 at concentrations above 4%. Also important is the capability of operation at high-temperatures in harsh industrial environments, aerospace, automotive, and power generation applications. Surface Acoustic Wave (SAW) technology offers many desirable properties for sensor fabrication, such as the capability of wireless and battery-free operation, mass-production, small size and weight. Piezoelectric substrates or thin films, such as langasite and aluminum nitrate, exist that allow SAW devices to operate at high temperatures. Langasite SAW-based devices have been previously demonstrated as temperature, strain and gas sensors. For high-temperature SAW-based gas sensors, sensitive films capable to react selectively with the target species are normally used. This work presents the detection of hydrogen gas at high-temperature (up to 470°C) using SAW resonators on the commercially available LGS plane described by Euler angles {0°, 138.5°,Ψ}. The Pt-Al_2O_3 composite thin film is used as both the electrode and sensitive layer. Devices fabricated along different crystal orientations on the same wafer revealed different sensitivities to H_2, which were also measured as a function of temperature up to 470°C. These different sensitivities to H_2 open the possibility of using different orientations of this commercially available LGS crystal cut to fabricate sensors capable of operating as a network, and detecting different measurands at high-temperature, including hydrogen gas.**

Keywords—Hydrogen gas sensor; High-temperature harsh-environment sensor; surface acoustic wave sensor; langasite orientations.

I. Introduction

The demand for reliable high-temperature hydrogen gas (H_2) and hydrocarbon sensors is steadily increasing as industry needs such devices to increase safety and energy-efficiency in monitoring and process control [1]. Industrial applications including petrochemical, steelmaking and power generation can all benefit from H_2 gas sensors. In addition, there is the need to store H_2 in volatile concentrations (4% to 90%), which requires H_2 sensors capable of withstanding high-temperature shocks and extended exposures in harsh environments [2]. Surface Acoustic Wave (SAW) devices present numerous advantages as a gas-sensing sensor platform, including wireless battery-free operation, robustness, small size and weight, and mass-fabrication capabilities using semiconductor industry processes [3]. SAW devices fabricated on langasite (LGS) have been successfully operated at temperatures above 800°C for over five months [4]. It has been previously demonstrated that SAW resonators (SAWRs) can be used as sensors for H_2 gas using a Pt film as the electrode up to 300°C [5].

In this work, SAWRs utilizing Pt-Al_2O_3 as electrodes have been used to demonstrate H_2 detection up to 471°C. Utilizing the electrodes as sensing elements for high temperature gas detection has the advantage of avoiding the use of additional layer or more complex structures [6]. Devices have been fabricated and tested for H_2 detection along four orientations of the commercially available LGS cut Euler angles {0°, 138.5°, Ψ}. The results have shown different sensitivities to H_2 for the different orientations measured from room temperature up to 471°C. These different sensitivities for different orientations and for a wide range of temperatures suggest the capability of using SAWRs fabricated along multiple orientations of the same plane in arrays or sensor networks to detect different measurands including gases at high temperatures.

II. Fabricated SAWRs & Experimental Setup

The SAWRs used in this work were fabricated on the commercially available LGS cut Euler angles {0°, 138.5°, Ψ} at the University of Maine Frontier Institute for Research in Sensor Technologies utilizing lift-off photolithography and e-beam deposition described in [7], [8]. In addition to Ψ=26.7°, devices were fabricated along three other orientations using the same mask at Ψ=14.7°, 32.7°, and 77.7° due to their temperature compensations around 175°C, room temperature, and 300°C, respectively [9]. All SAWRs employed the Pt-Al_2O_3 film composite discussed in [7]-[9], with 82% Pt and 18% Al_2O_3, and have interdigital transducers (IDTs) and reflector electrodes fabricated with 1:1 mark to space ratio. Table I lists additional SAWR characteristics for the different orientations. All the SAWRs were designed to operate around 190MHz. After fabrication, the wafers were cleaned (acetone, iso-propanol, methanol, de-ionized (DI) water, dried in N_2 stream), prior to the

Table I. Device-specific fabrication parameters.

Orientation	2*p (μm) p=electrode periodicity	Number of IDT electrodes	Power Flow Angle, PFA (°)	Acoustic Aperture W (wavelengths)
14.7°	13.4	241	26	61
26.7°	14	161	0	51
32.7°	14	161	-3	51
77.7°	13.1	241	-16	61

This work has been funded by the U.S. Department of Energy/National Energy Technology Laboratory (NETL) under grant number DE-FE0026217

annealing of the Pt-Al_2O_3 electrode in an alumina crucible to 800°C for four hours [7]-[9]. The wafers were then diced to an approximate dimension of 10 x 3 x 0.5mm^3.

Fig. 1 shows the experimental setup used for this work. Fig. 1a shows the two-chamber stainless steel box used for the high-temperature gas-cycling testing of SAWRs reported in this paper. Each chamber has dimensions of 57 x 24 x 12.5 mm^3 and was used to house two LGS SAWRs and one K-type thermocouple (TC). The SAWRs fabricated along Ψ=14.7° and 77.7° are housed in one chamber, and the SAWRs fabricated along Ψ=26.7° and 32.7° in the other, each chamber containing its respective thermocouple. The SAWRs were held inside the chamber by 4mil Pt wire, and 1 mil Pt wire was used to provide electrical connections between the high-temperature coaxial cables and the SAWRs. The Pt wires were all welded using a Unitek resistance welder. The TCs on each chamber were mounted on top of a piece of LGS to mimic the temperature seen by the SAWRs.

Fig. 1b shows the block diagram of the data acquisition system utilized. An automated gas delivery system consisting of three three-way Advanced Pressure Technology (AP Tech) valves and two independent Tylan mass-flow controllers (one for each chamber) with a capacity of 1 standard liter per minute was used to deliver high purity N_2 gas (>99.999%) (henceforth referred to as N_2), 4.7 grade O_2 (henceforth O_2) and a 4%/96% H_2/N_2 mixture (henceforth H_2). All gases discussed in these tests

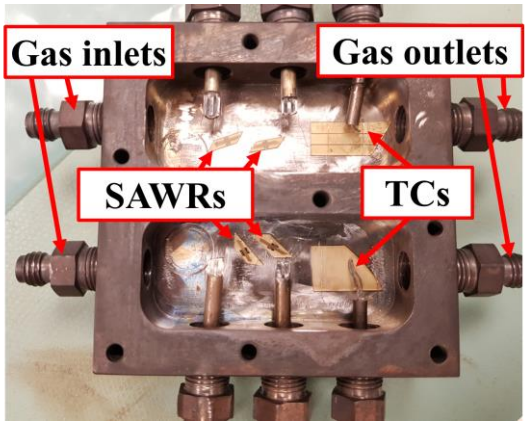

(a)

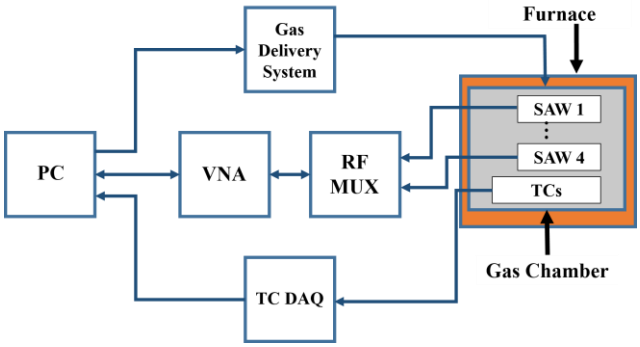

(b)

Fig. 1. Experimental Setup. a) High-temperature stainless-steel box containing devices and thermocouples; b) schematic for data acquisition and gas delivery.

were delivered with a flow rate of 950sccm. The devices were heated using a Thermolyne 6000 Furnace. An E5071C Vector Network Analyzer (VNA) in conjunction with a Mini-Circuits 4-way RF switch (RF MUX) were used for SAWR interrogation. A frequency sweep of 10MHz centered at 190MHz with 2001 points and an Intermediate Frequency (IF) bandwidth of 5kHz was used in order to be able to interrogate four devices four times in under a minute. Parabolic fitting over a bandwidth of 25kHz was implemented to extract the peak of each SAWR resonant frequency. The temperature was recorded before and after each device was interrogated and both temperatures averaged to associate a temperature to each frequency sweep. After a change in gas species, all four devices were interrogated every 15 seconds for five minutes, totaling 20 measurements for each device during the five-minute period. After those measurements, all four devices were interrogated once every 5 minutes during periods of constant gas flow until the next change in gas species, when the measurement procedure repeated.

Prior to the gas testing up to 471°C reported in the next section, the frequency dependency with temperature for the SAWRs oriented along Ψ=14.7°, 26.7°, 32.7°, and 77.7° were obtained. This work was done to assess the influence of possible temperature variations or fluctuations in the gas readings. The SAWRs temperature dependence was extracted in a constant N_2 flow by subjecting the setup to increments of 20°C from 60°C to 480°C and held at temperature for 2 hours, while the sensors were interrogated every 5 minutes. The average resonant frequency at each temperature was taken after one hour had transpired giving 12 measurements per temperature step. A 2^{nd} degree polynomial approximation was used to extrapolate the results to the range between 0 and 500°C. Fig. 2a plots the average data measured for the orientations used, normalized to the maximum measured value of frequency for that orientation $f_{0ΨT}$. Fig. 2b shows the respective temperature sensitivity curves.

The devices were tested at the following discrete furnace setup temperature: room temperature (no heating, furnace off), 100°C, 200°C, 300°C, 400°C, and 500°C. These values correspond to the following actual temperature in the chambers averaged from measurements by the TCs in both chambers throughout the entire test after reaching a stable temperature: 21°C, 91°C, 186°C, 276°C, 373°C and 471°C, respectively.

III. Results and Discussion

Fig. 3 shows the measured resonant frequency response (left vertical axis) of an SAWR oriented along Ψ = 26.7° and operated around 186°C (right vertical axis) as a function of time under exposure to N_2, O_2 and H_2, as shown at the bottom of the plot (also right vertical axis). The test started with an initialization sequence (Feature A) consisting of N_2 flow while the setup reaches a stable temperature, and an initial oxidation period of three 20-min O_2 and N_2 cycles, followed by an hour period in N_2 as a purging period. Features B, D and F are reduction periods consisting of four 20-min H_2 and four 20-min N_2 cycles followed by a 1-hour purging period in N_2. Features C and E are oxidation periods consisting of four 20-min O_2 and four 20-min N_2 cycles followed by an hour purging period in N_2. This plot is intended as an example of the gas exposure tests carried out and measurements taken for all the orientations and

at the different temperatures reported in this section. The frequency shift labeled as Δf_1 in Fig. 3 is due to the first 20-min exposure to H_2 after oxidation Period C. Similarly, Δf_2 was recorded after oxidation Period E. The resonant frequency at the end of the first 20-min exposure to H_2 after oxidation Period C was adopted as the reference frequency for that test at that particular temperature, and labeled f_{0i}, varying for different temperatures and orientations.

Table II lists the values of Δf_1 and Δf_2 for the different LGS SAWR orientations grouped at the same test temperatures, giving also the reference frequency f_{0i} measured for each orientation at each particular temperature. Fig. 4 plots the average of Δf_1 and Δf_2 normalized by the respective resonant frequency f_{0i} as a function of temperature for the different LGS SAWR orientations analyzed.

As can be seen from Fig. 4, there is a marked difference in frequency variation due to the insertion of H_2 for the different orientations analyzed. From weaker to stronger frequency response to H_2 the orientations can be ordered as: Ψ=77.7°, 14.7°, 32.7° and 26.7°. This order remained true from room temperature all the way to the maximum temperature measured. The data points at 471°C for Ψ=26.7° and 32.7° are missing in Table II and Fig. 4, since the readings for both devices in this chamber presented inconsistencies, possibly due to failure in the steel box cover sealing or gas system delivery for this chamber.

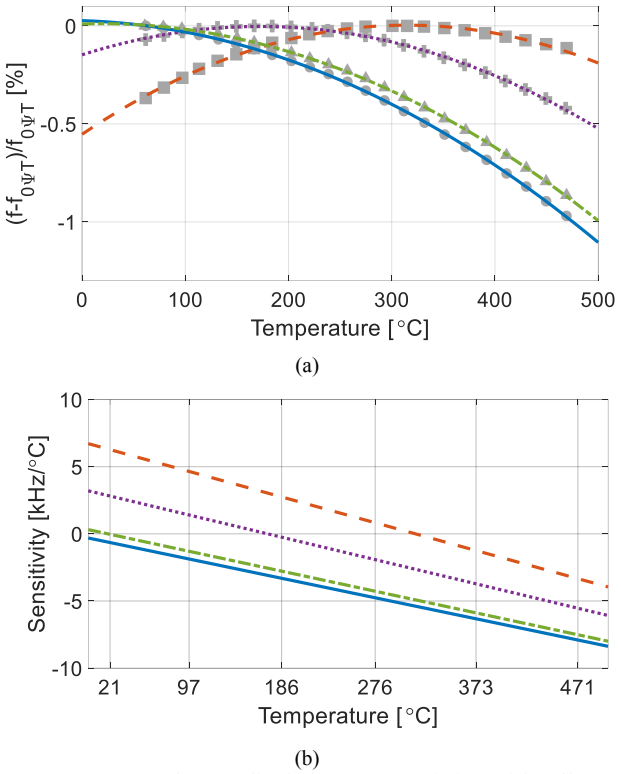

Fig. 2. a) Measured normalized frequency variation $(f-f_{0\Psi T})/f_{0\Psi T}$ vs. temperature for the LGS orientations used and polynomial fit; b) calculated sensitivity. Ψ = 77.7°: squares dashed red line; Ψ = 14.7°: crosses dotted purple line; Ψ = 32.7°: triangles dotted/dashed green line; Ψ = 26.7°: circles solid blue line. For the orientations 77.7°, 14.7°, 26.7° and 32.7° the value of $f_{0\Psi T}$ is 189.927,191.075, 191.934, 191.465MHz respectively.

Fig. 5 plots the calculated SAW electromechanical coupling coefficient (K^2=100 $|v_{free}-v_{met}|/v_{met}$) using the constants from [10]. Comparing the results shown in Fig. 4 and the respective K^2 for each orientation, there seems to be a correlation between the intensity of K^2 and the intensity of the response to H_2, with exception to Ψ = 77.7° and 14.7°, where the order is reversed. Considering that the calculated K^2 for Ψ = 77.7° and 14.7° differ by about 2% only, it is unclear at this point whether the reverse order is due to imprecision in device orientation during fabrication, discrepancy in the piezoelectric coefficients used, or yet other variables such as the electrode reflection coefficient,

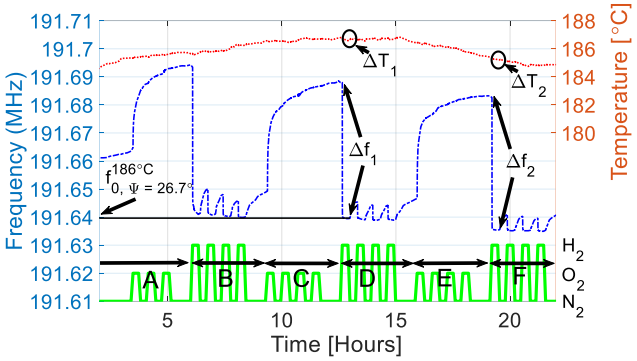

Fig. 3. Resonant frequency plotted as a function of gas exposure for Ψ =26.7° at ~186°C for one round. The dotted line is the temperature recorded with the thermocouple. Δf_1 and Δf_2 are the recorded frequency shifts after the first 20-min exposure to H_2 after an oxidation period (B and D). f_0 is the reference frequency for the temperature, defined as the frequency after Δf_1.

Table II. Tabulated summary of results. f_{0i} is the adopted reference frequency at each temperature, and Δf_1 and Δf_2 are the frequency shifts as shown in Fig. 4.

Orientation	f_{0i} (MHz)	Δf_1 (kHz)	Δf_2 (kHz)	Max. ΔT_i (°C)	Sensit. (kHz/°C)	Max. $\Delta f_T/f_{0i}$ [%]
21°C						
77.7°	188.962	4	5	-0.61	6.2	-0.002
14.7°	190.476	11	11	-0.61	2.8	-0.0009
26.7°	191.929	28	28	-0.24	-0.7	0.00009
32.7°	191.436	22	23	-0.24	-0.1	0.00001
97°C						
77.7°	189.431	5	5	-0.36	4.6	-0.0009
14.7°	190.685	12	11	-0.36	1.4	-0.0003
26.7°	191.886	35	32	-0.17	-1.8	0.0002
32.7°	191.441	29	27	-0.17	-1.3	0.0001
186°C						
77.7°	189.776	9	8	-0.4	2.7	-0.0006
14.7°	190.743	20	20	-0.4	-0.2	0.00004
26.7°	191.640	48	47	-0.24	-3.3	0.0004
32.7°	191.251	42	40	-0.24	-2.8	0.0004
276°C						
77.7°	189.924	16	16	-0.35	0.7	-0.0001
14.7°	190.621	37	38	-0.35	-1.9	0.0003
26.7°	191.215	85	86	-0.34	-4.8	0.0009
32.7°	190.882	73	72	-0.34	-4.3	0.0008
373°C						
77.7°	189.860	27	26	-0.75	-1.3	0.0005
14.7°	190.299	58	58	-0.75	-3.8	0.001
26.7°	190.579	137	137	-0.59	-6.3	0.002
32.7°	190.314	106	105	0.59	-5.9	-0.002
471°C						
77.7°	189.695	25	28	-0.48	-3.3	0.0009
14.7°	189.904	58	59	-0.48	-5.5	0.001
26.7°	190.045	NA	NA	-0.56	-7.8	0.002
32.7°	189.772	NA	NA	-0.56	-7.5	0.002

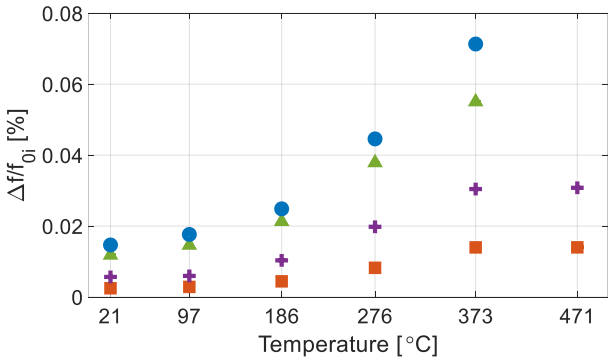

Fig. 4. Measured relative frequency variation due to H_2 exposure at the measured temperatures for Ψ = 77.7° (orange squares); Ψ = 14.7° (purple +); Ψ = 26.7° (blue circles); and Ψ = 32.7° (green triangles). Note: f_{0i} value varies with each temperature point as described in the text and shown in Table II.

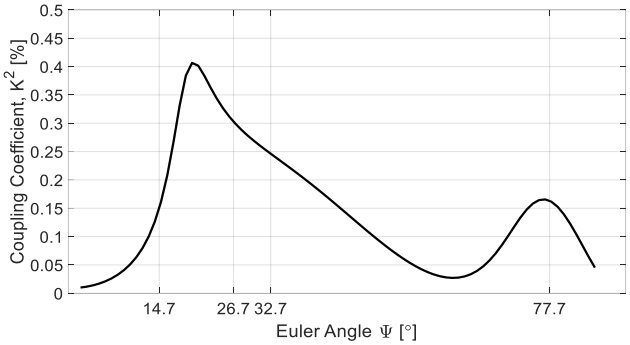

Fig. 5. Calculated SAW electromechanical coupling coefficient K^2 for the LGS Euler angles (0°, 138.5°, Ψ). The orientations of interest are marked on the x-axis.

which played a role in making the Ψ = 14.7° have a stronger response to H_2 when compared to Ψ =77.7°. As a final note, ΔT_1 and ΔT_2 shown in Fig. 3, which represents the temperature variation due to the switching from the N_2 gas to the 4%/96% H_2/N_2 mixture, could compromise the frequency variation results due to exposure to H_2 in Fig. 4. The measured temperature variation by the TCs (orange temperature curve in Fig. 3) between the time the frequencies were measured to obtain Δf_i was dependent on temperature. For the measured temperatures 21°C, 91°C, 186°C, 276°C, 373°C and 471°C the respective maximum ΔT_i were: -0.5°C, -0.3°C, -0.2°C, -0.4°C, -0.6°C, and -0.7°C. Using the sensitivity curve given in Fig. 2, the maximum temperature induced frequency variation is listed in Table II, which are smaller than the shapes used to plot Fig. 4.

IV. Conclusion

This work has presented the detection of H_2 by LGS SAWRs fabricated along four orientation of the commercially available LGS wafer Euler angles {0°,138.5°,Ψ}, Ψ=14.7°, 26.7°, 32.7°, and 77.7° at temperatures up to 471°C. The hydrogen in the 4%/96% H_2/N_2 mixture was successfully detected by all orientations at all temperatures, but different sensitivities to H_2 were observed for different orientations. The sensitivities seem to correlate to the electromechanical coupling and potentially to other SAWR design and propagation parameters. Variations in temperature during the measurements have been considered, and do not seem to have impacted the results observed. These findings suggest that devices oriented along different orientations can be used in arrays or sensor networks to distinguish between different measurands or different gases concentrations at high temperatures.

Disclaimer

This work was supported by U.S. Department of Energy Award #: DE-FE0026217. Disclaimer: This report was prepared as an account of work sponsored by an agency of the United States Government. Neither the United States Government nor any agency thereof, nor any of their employees, makes any warranty, express or implied, or assumes any legal liability or responsibility for the accuracy, completeness, or usefulness of any information, apparatus, product, or process disclosed, or represents that its use would not infringe privately owned rights. Reference herein to any specific commercial product, process, or service by trade name, trademark, manufacturer, or otherwise does not necessarily constitute or imply its endorsement, recommendation, or favoring by the United States Government or any agency thereof. The views and opinions of authors expressed herein do not necessarily state or reflect those of the United States Government or any agency thereof.

References

[1] S. Akbar, P. Dutta, and C. Lee, "High-Temperature Ceramic Gas Sensors : A Review," *Int. J. Appl. Ceram. Technol.*, vol. 311, no. x, pp. 302–311, 2006.

[2] A. Trinchi, S. Kandasamy, and W. Wlodarski, "Chemical High temperature field effect hydrogen and hydrocarbon gas sensors based on SiC MOS devices," *Sensors Actuators, B Chem.,* vol. 133, pp. 705–716, 2008.

[3] J. Devkota, P. R. Ohodnicki, and D. W. Greve, "SAW sensors for chemical vapors and gases," *Sensors (Switzerland)*, vol. 17, no. 4, pp. 801–828, 2017.

[4] M. Pereira da Cunha, T. Moonlight, R. Lad, D. Frankel, and G. Bernhardt, "High Temperature Sensing Technology for Applications Up To 1000°C," in *IEEE Sensors Conference*, 2008, pp. 752–755.

[5] J. A. Thiele and M. Pereira da Cunha, "High temperature LGS SAW gas sensor," *Sensors Actuators, B Chem.*, vol. 113, no. 2, pp. 816–822, Feb. 2006.

[6] P. Zheng *et al.*, "Langasite SAW device with gas-sensitive layer," in *Proceedings - IEEE Ultrason. Symp.*, 2010, pp. 1462–1465.

[7] Frankel, S. C. Moulzolf, M. Pereira da Cunha, and R. J. Lad, "Influence of composition and multilayer architecture on electrical conductivity of high temperature Pt-alloy films," *Surf. Coatings Technol.*, vol. 284, pp. 215–221, 2015.

[8] A. Maskay, A. Ayes, and M. Pereira da Cunha, "Stability of Pt/Al2O3-based electrode langasite SAW sensors with Al2O3 capping layer and yttria-stabilized zirconia sensing layer," *IEEE Int. Ultrason. Symp. IUS*, 2017, pp. 2–5.

[9] A. Ayes, A. Maskay and M. Pereira da Cunha, "Predicted and measured temperature compensated surface acoustic wave devices for high-temperature applications" *Electronics Letters,* vol. 53, no. 11, pp. 699-700, 2017.

[10] P. Nicolay and T. Aubert, "A numerical method to derive accurate temperature coefficients of material constants from high-temperature SAW measurements: Application to langasite," *IEEE Trans. Ultrason. Ferroelectr. Freq. Control*, vol. 60, no. 10, pp. 2137–2141, 2013.